

## Article

# The Morphology-Controllable Synthesis of Ni–Co–O Nanosheets on a 3D Porous Ni Template as a Binder-Free Electrode for a Solid-State Symmetric Supercapacitor

Han-Wei Chang <sup>1,2,\*</sup> , Chia-Hsiang Lee <sup>1</sup>, Yu-Xiang Hong <sup>1</sup>, Jeng-Lung Chen <sup>3</sup>, Jin-Ming Chen <sup>3</sup> and Yu-Chen Tsai <sup>4,\*</sup>

<sup>1</sup> Department of Chemical Engineering, National United University, Miaoli 360302, Taiwan; tonylee36987412@gmail.com (C.-H.L.); jennis10130103@gmail.com (Y.-X.H.)

<sup>2</sup> Pesticide Analysis Center, National United University, Miaoli 360302, Taiwan

<sup>3</sup> National Synchrotron Radiation Research Center, Hsinchu 30076, Taiwan; chen.jl@nsrc.org.tw (J.-L.C.); jmchen@nsrc.org.tw (J.-M.C.)

<sup>4</sup> Department of Chemical Engineering, National Chung Hsing University, Taichung 40227, Taiwan

\* Correspondence: hwchang@nuu.edu.tw (H.-W.C.); yctsai@dragon.nchu.edu.tw (Y.-C.T.); Tel.: +886-37-382216 (H.-W.C.); +886-4-22857257 (Y.-C.T.)

**Abstract:** In this work, a porous Ni template (Ni–Co–O@3D Ni) with Ni–Co oxide nanosheets (Ni–Co–O)@3D was synthesized by incorporating Ni–Co oxide nanosheets within a 3D porous Ni template as a binder-free electrode for a supercapacitor. The 3D Ni template was synthesized with hydrogen bubble templates that possessed different applied voltages that marked differences in terms of physicochemical properties, as well as factors that affect the subsequent growth of Ni–Co–O nanosheets. Then, Ni and Co metal ion sources were introduced to produce the morphology adjustment of Ni–Co–O@3D Ni with a multiple hierarchical architecture with a hydrothermal process. Field emission scanning electron microscopy (FESEM), X-ray absorption spectroscopy (XAS), and an electrochemical analysis were employed to investigate the morphological, structural, and electrochemical characteristics. FESEM and XAS results evidenced that Ni–Co–O@3D Ni consists of a 3D, well-designed hierarchical interconnected network, and the local electronic structure change has a great influence on the capacitive performance. The electrochemical results of Ni–Co–O@3D Ni displayed an excellent electrochemical performance due to the synergistic effect of Ni and Co on Ni–Co–O@3D Ni, which possessed multiple oxidation states to enable various reversible Faradaic redox reactions. Remarkably, the solid-state symmetric supercapacitor fabricated with Ni–Co–O@3D Ni exhibited excellent capacitive behaviour at a wide operating voltage window and cycling performance. Also, the as-assembled solid-state symmetric supercapacitor (two devices in series) can successfully illuminate a desired parallel pattern consisting of 36 red LED lights, demonstrating its practical application as a supercapacitor.

**Keywords:** Ni–Co oxide nanosheets; 3D porous Ni template; solid-state symmetric supercapacitor



**Citation:** Chang, H.-W.; Lee, C.-H.; Hong, Y.-X.; Chen, J.-L.; Chen, J.-M.; Tsai, Y.-C. The Morphology-Controllable Synthesis of Ni–Co–O Nanosheets on a 3D Porous Ni Template as a Binder-Free Electrode for a Solid-State Symmetric Supercapacitor. *Energies* **2023**, *16*, 5467. <https://doi.org/10.3390/en16145467>

Academic Editor: Claudio Mele

Received: 19 June 2023

Revised: 9 July 2023

Accepted: 13 July 2023

Published: 19 July 2023



**Copyright:** © 2023 by the authors. Licensee MDPI, Basel, Switzerland. This article is an open access article distributed under the terms and conditions of the Creative Commons Attribution (CC BY) license (<https://creativecommons.org/licenses/by/4.0/>).

## 1. Introduction

Supercapacitors, as promising energy storage devices, have attracted a great research interest due to their high power density, fast charge/discharge rate, excellent reversibility, and high durability [1,2]. They can be integrated into hybrid energy storage systems to meet the demand for renewable energy sources in addressing climate change and a sustainable environment. Suitable electrode materials play a decisive role in the electrochemical performance of supercapacitors. Thus, the exploration of electrode material design strategies provides the basic guideline for developing the future trends of supercapacitor technology. The most common method of fabricating electrode materials, using a thin film preparation technique with the addition of a polymer binder and a conductive

additive, improves their adhesion strength and electrode activation, thereby preserving the mechanical and electronic properties of electrode materials. Moreover, the addition of an insulating binder aggravates the problem of contact resistance and increases the internal resistance of electrode materials, which results in a decreased specific capacity and rate performance, limiting their practical application in supercapacitors. To overcome this, a three-dimensional (3D) conductive substrate with a micro/nano architectural design and interconnected open network structure is able to act as a conductive template for the following growth of active materials [3,4]. Constructed active materials that are directly grown onto a 3D conductive substrate are expected to have a larger specific area as well as electroactive sites, which should enhance fast ion/electron transport that occurs at the electrode/electrolyte interface, exhibiting excellent supercapacitive performance. In this regard, transition metals, such as iron (Fe), copper (Cu), zinc (Zn), and nickel (Ni), with integrated advantages of an earth-abundant, high-level electrical conductivity; strong substrate interaction; and good mechanical ductility may be good choices to construct the conductive substrate. In particular, Ni-based conductive substrates have attracted increasing attention due to a low cost, excessive electrical conductivity, high stability, and great alkali corrosion resistance [4,5]. Various synthesis methods have been reported to prepare a 3D Ni interconnected structure within a conductive substrate with controllable design and synthesis strategies, including the chemical deposition method [6], electrochemical deposition method [7], magnetic-field-assisted chemical reduction method [8], electron-beam evaporation method [9], and aerosol-assisted chemical vapor deposition [10]. Such a 3D interconnected conductive substrate could provide a large electric contact surface to serve as both anchoring sites and electrocatalytically active sites for the nucleation and conformal growth of active materials with interconnected networks and an additional pseudocapacitance contribution to the overall capacitance performance. Simultaneously, the anchoring of active materials on the surface of a 3D conductive substrate with continuously interconnected conductive networks enables intimate interface contact between electrode/electrolyte interfaces for a fast electron transfer that could improve electron transport and enhance electrolyte diffusion efficiency, which would result in a significant enhancement of electrochemical kinetics [11,12].

Pseudocapacitance is contributed by pseudocapacitive materials via Faradaic processes involving surface or near-surface redox reactions. Among a variety of pseudocapacitive materials, binary (Mn, Cu, Zn, Co, Ni, etc.) and ternary (Cu-Co, Mn-Co, Zn-Co, Ni-C, etc.) transition metal oxides generally possess rich redox chemistry and valence state transitions, which offer ideal pseudocapacitance. At the same time, these transition metal oxides could be easily converted into hierarchical electrocatalyst layers, allowing good conformal growth on the surface of 3D interconnected conductive substrates. In contrast, ternary transition metal oxides possess multiple oxidation states that enhance multiple redox reactions during electrochemical reactions to induce pseudocapacitive behaviour and, therefore, exhibit a better supercapacitive performance than binary transition metal oxides [13,14].

In this work, the morphology-controllable synthesis of ternary Ni-Co-O nanosheets grown on the porous structure of a 3D Ni template (Ni-Co-O@3D Ni) is directly used as a binder-free electrode for solid-state symmetric supercapacitors. A 3D Ni template has a tunable physicochemical characterization, which is adjusted with hydrogen bubble templates possessed for different applied voltages. Furthermore, the hydrothermal method has been employed to synthesize ternary Ni-Co-O nanosheets within a 3D Ni template. A 3D Ni template can be used as a support substrate for the growth of Ni-Co-O nanosheets to obtain different morphologies of Ni-Co-O@3D Ni. The supercapacitor constructed with the morphology adjustment of Ni-Co-O@3D Ni can largely boost electrode performance for an application in electrochemical energy storage devices, benefiting from the strong synergistic effect between Ni-Co-O and 3D Ni. The encouraging results indicate that the design of Ni-Co-O@3D Ni could lead to promising materials for practical usage as a solid-state symmetric supercapacitor.

## 2. Materials and Methods

### 2.1. Reagents

Nickel(II) chloride hexahydrate ( $\text{NiCl}_2 \cdot 6\text{H}_2\text{O}$ ), nickel(II) nitrate hexahydrate ( $\text{Ni}(\text{NO}_3)_2 \cdot 6\text{H}_2\text{O}$ ), cobalt(II) nitrate hexahydrate ( $\text{Co}(\text{NO}_3)_2 \cdot 6\text{H}_2\text{O}$ ), poly(vinyl alcohol) (PVA), ammonium chloride ( $\text{NH}_4\text{Cl}$ ), potassium hydroxide (KOH), and urea were purchased from Sigma-Aldrich (St. Louis, MO, USA). All chemicals used were of analytical grade and were used as received without further purification. All chemical solutions were prepared with a Milli-Q water purification system (Millipore, Milford, MA, USA).

### 2.2. Preparation of Ni–Co–O@3D Ni

The porous 3D-Ni template was synthesized during Ni electrodeposition on the Ni wire (diameter of 0.25 mm) using hydrogen bubble templates (according to our previous research work [1]). First, Ni wire was carefully cleaned sequentially with 1 M HCl, ethanol, and DI water under ultra-sonication three times for 15 min each to remove residues and dried at 100 °C for the next test. Then, a two-electrode cell containing Ni wire as a cathode and Pt as an anode was immersed into a mixture of 2 M  $\text{NH}_4\text{Cl}$  and 0.2 M  $\text{NiCl}_2 \cdot 6\text{H}_2\text{O}$  in deionized (DI) water as an electrolyte, and the mixture was used to prepare the porous 3D-Ni template using hydrogen bubble templates for different applied voltages (4, 5, and 6 V). The resulting samples were designated as 3D Ni- $x$  ( $x = 4, 5,$  and  $6$ ). Subsequently, the Ni-Co oxides (Ni–Co–O) on 3D Ni- $x$  was prepared using hydrothermal method. Briefly, 0.3 mmol  $\text{Ni}(\text{NO}_3)_2 \cdot 6\text{H}_2\text{O}$ , 0.3 mmol  $\text{Co}(\text{NO}_3)_2 \cdot 6\text{H}_2\text{O}$ , and 1.8 mmol urea were first dissolved in the mixed solution of 30.0 mL DI water and 10.0 mL ethanol to obtain a homogeneous suspension and then transferred into a 100 mL Teflon-lined stainless-steel autoclave. After that, 3D Ni- $x$  was put into an autoclave at 120 °C for 2 h. Finally, the Ni-Co oxide nanosheets (Ni–Co–O) grown on 3D Ni- $x$  were taken out and washed with DI water thrice for 15 min each, dried in an oven to remove the remaining reagents, and collected for subsequent characterization. The obtained Ni-Co oxides (Ni–Co–O) grown on 3D Ni- $x$  were designated as Ni–Co–O@3D Ni- $x$  ( $x = 4, 5,$  and  $6$ ) (ca. 0.43 mm diameter). The synthesis route is schematically illustrated in Figure 1. For comparison, the Ni–Co–O@3D Ni- $x$  sample was synthesized under the same experimental procedure and subsequent thermal annealing at 300 °C and may offer insight into the correlation of the thermal annealing-induced phase transformation for the synthesized and post-annealed (for comparison) Ni–Co–O@3D Ni- $x$  sample.

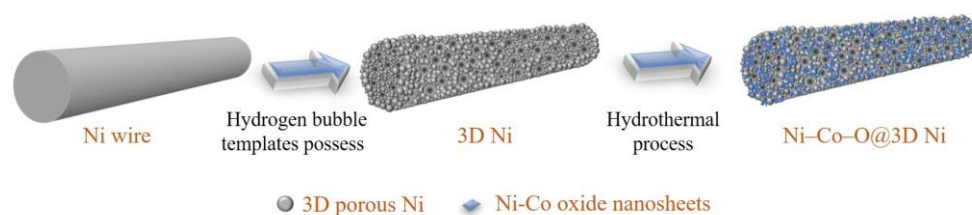


**Figure 1.** Schematic illustration of the synthesis of Ni–Co–O@3D Ni.

### 2.3. Fabrication of Solid-State Symmetric Supercapacitors

The solid-state symmetric supercapacitor was assembled by employing potassium hydroxide-poly(vinyl alcohol) (KOH–PVA) gel electrolyte and two Ni–Co–O@3D Ni- $x$  electrodes. The KOH–PVA gel electrolyte was made by adding 1 g of PVA in 10 mL of 1 M KOH and stirred at 85 °C until it became clear. Then, two Ni–Co–O@3D Ni- $x$  electrodes were submerged in the gel electrolyte for about 30 min at room temperature. After that, two gel-coated Ni–Co–O@3D Ni- $x$  electrodes were assembled in parallel and left overnight under ambient conditions until the electrolyte solidified to obtain a solid-state symmetric supercapacitor.

#### 2.4. Characterization

The morphology was characterized using a field emission scanning electron microscope (FESEM, JSM-7800F, JEOL, Akishima, Japan). Synchrotron X-ray absorption spectroscopy (XAS) (for the Ni, Co K-edges, and Ni, Co L-edges) was used at beamlines BL20A and BL17C of the National Synchrotron Radiation Research Center (NSRRC, Hsinchu, Taiwan) and operated with an energy of 1.5 GeV and a maximum stored current of 300 mA. Electrochemical measurements were performed using either a two- or three-electrode system of an electrochemical analyser (Autolab, model PGSTAT30, Eco Chemie, Utrecht, The Netherlands). The as-synthesized Ni-Co-O@3D Ni-x was analysed with two different electrochemical measuring techniques (cyclic voltammetry (CV) and galvanostatic charge-discharge (GCD)). In the three-electrode system, the supercapacitor comprised a Ni-Co-O@3D Ni-x working electrode, a platinum wire counter electrode, and an Ag/AgCl (3 M KCl) reference electrode. All electrochemical measurements were recorded in 1 M KOH aqueous solution within the potential window from 0.0 to 0.45 V versus Ag/AgCl. In the two-electrode system, the solid-state symmetric supercapacitor consisted of two Ni-Co-O@3D Ni-x electrodes and KOH-PVA gel electrolyte within the potential window from 0.0 to 1.6 V.

### 3. Results

The surface morphologies of the three-dimensional (3D) Ni-x and Ni-Co-O@3D Ni-x samples were characterised using field emission scanning electron microscopy (FESEM) at two magnifications: 500 $\times$  and 30,000 $\times$ . Figure 2a–c show low-magnification (500 $\times$ ) FESEM images of the 3D porous Ni structures on the Ni wire (3D Ni-x) obtained by the utilization of hydrogen bubble templates. The low-magnification FESEM images provide insights into the surface structures of the Ni wire with 3D Ni-x and Ni-Co-O@3D Ni-x samples. The porous and interconnected structures on the Ni wire became more pronounced with increasing applied voltage. The pores exhibit diameters ranging from sub-micrometres to several micrometres. Upon closer examination using high-magnification FESEM (Figure 2d–f), the surface of the 3D porous Ni structures on the Ni wire appears denser and exhibits a more uniform rough structure, which is particularly evident in the 3D Ni-6 sample. This results in a larger specific surface area, making it an ideal growth template for the subsequent hydrothermal growth of Ni-Co oxides. As a result, the low-magnification FESEM images in Figure 3a–c confirm the dense and uniform coverage of Ni-Co oxides across the entire substrate of the 3D Ni-x samples. Furthermore, the high-magnification FESEM images (Figure 3d–f) demonstrate the interconnected growth of these Ni-Co oxides, forming a well-defined interconnected network structure on the 3D Ni-x sample substrate. Interestingly, some of the Ni-Co oxides develop into ultrathin nanosheets along the surface of the 3D Ni-x sample substrate to interconnect the 3D Ni interconnected network structure, which shows the potential to construct Ni-Co-O@3D Ni-x samples with multiple hierarchical architectures. Figure 3g–i provide a magnified view of the 3D multiple hierarchical architecture by zooming in on the yellow-framed areas of Figure 3d–f. These magnified FESEM images clearly illustrate that the well-defined interconnected network structure on the 3D Ni-x sample substrate is formed by a well-ordered array of nanosheets, resulting in a large specific surface area. The thickness of the Ni-Co-O nanosheet increases significantly with increasing applied voltages, ranging from several nanometres to several tens of nanometres. Notably, the Ni-Co-O nanosheets in the Ni-Co-O@3D Ni-6 samples appear to consist of sandwiched layers (2–3 layers of Ni-Co-O nanosheets) (see Figure 3i), creating numerous open spaces and convenient channels. This leads to an increased number of electroactive sites in the Ni-Co-O@3D Ni-6 samples and is expected to further accelerate species diffusion and electron/ion transport, ultimately improving their electrochemical performance [15]. The formation of Ni-Co-O@3D Ni is further confirmed by XRD and energy-dispersive X-ray (EDX) analysis, as shown in Figures S1 and S2 in the Supplementary Materials. Figure S1 displays the XRD patterns of 3D Ni, Ni-Co-O@3D Ni, and Ni-Co-O@3D Ni annealed at 300 °C. Notably, all XRD

patterns show clear peaks corresponding to metallic Ni (marked with  $\diamond$ ), originating from the 3D Ni structures on the nickel substrate. During the hydrothermal preparation of Ni-Co-O@3D Ni, no new peaks indicating the formation of a crystalline phase appear in the XRD pattern. This suggests the presence of an amorphous phase comprising the Ni-Co-O matrix. However, it can be observed that a new phase starts to appear, which allows the characterisation of the phase transformation into a new phase by annealing Ni-Co-O@3D Ni at 300 °C, which is believed to be due to the presence of Ni-Co components [16,17]. The EDX analysis, shown in Figure S2, confirms the presence of Ni, Co, and O elements in the prepared Ni-Co-O@3D Ni samples, without any significant impurities. These results from XRD and EDX analyses in Figures S1 and S2 reflect the successful synthesis of Ni-Co-O@3D Ni samples without impurities. For further detailed characterisation of the 3D Ni-x and Ni-Co-O@3D Ni-x samples, X-ray absorption spectroscopy (XAS) measurements were performed.

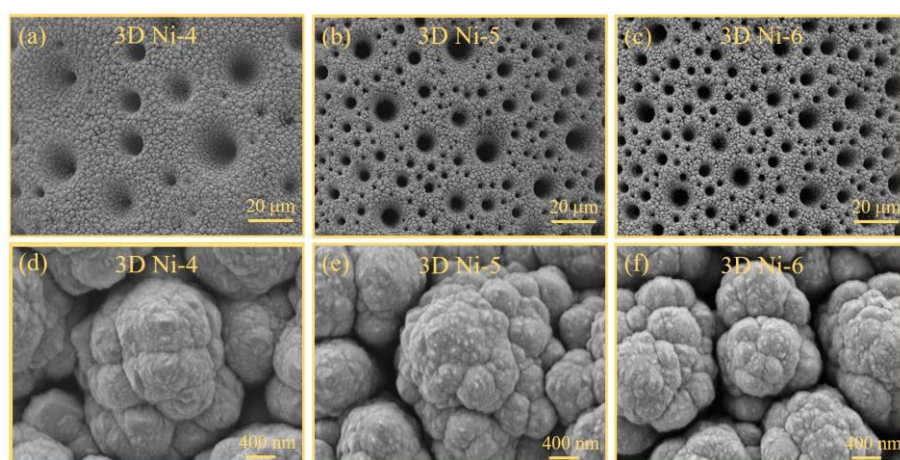


**Figure 2.** FESEM images of (a,d) 3D Ni-4, (b,e) 3D Ni-5, and (c,f) 3D Ni-6 at different magnifications.

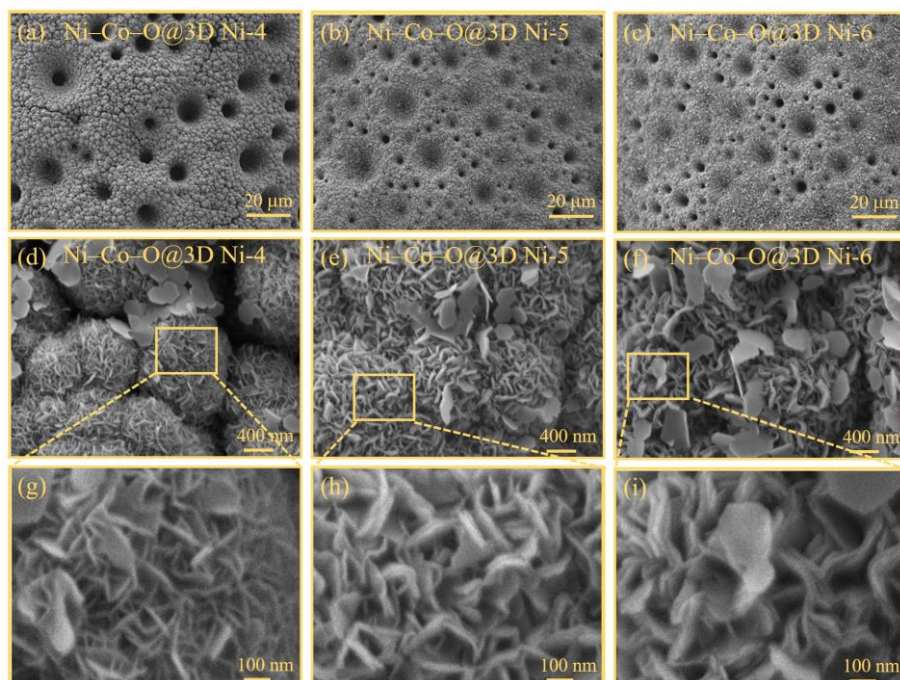


**Figure 3.** FESEM images of (a,d) Ni-Co-O@3D Ni-4, (b,e) Ni-Co-O@3D Ni-5, and (c,f) Ni-Co-O@3D Ni-6 at different magnifications. (g–i) The enlarged area of the marked place in Figure (d–f).

To obtain information on the electronic and structural properties of the 3D Ni-*x* and Ni-Co-O@3D Ni-*x* samples, XAS analysis was performed. XAS is a powerful tool for extracting information on electronic structure variations in complex coordination environments around target elements with different matrices, which is directly related to electrochemical performance. Figure 4 shows the Co and Ni K-edge XAS spectra of the Ni-Co-O@3D Ni-*x* samples, which were further analysed by comparing them with a series of standard samples, including a Ni foil, Ni oxide (NiO), and Co oxides (CoO and Co<sub>3</sub>O<sub>4</sub>). The Co K-edge XAS spectra in Figure 4a show a weak pre-edge absorption feature (the pre-edge region is magnified in the inset) and a strong main absorption feature. The inset in Figure 4a shows the pre-edge regions of the Co K-edge XAS spectra after background subtraction. The pre-edge absorption feature can be attributed to the dipole-forbidden transition from the transition metal 1s to the empty 3d states. Changes in the position and intensity of the pre-edge peak provide valuable information on the oxidation state of the sample and local structural symmetry. The most intense pre-edge features are generally caused by pure electric quadrupole coupling and/or 3d–4p orbital mixing arising from the non-centrosymmetric environment of the slightly distorted octahedral-based rhombohedral ground state [18]. In CoO, Co<sup>2+</sup> occupies octahedral sites (Co<sup>2+</sup> (Oh)) in a centrosymmetric arrangement. Co<sub>3</sub>O<sub>4</sub> has a normal spinel structure, with Co<sup>2+</sup> occupying tetrahedral sites (Co<sup>2+</sup> (Td)) and Co<sup>3+</sup> occupying octahedral sites (Co<sup>3+</sup> (Oh)). Co<sub>3</sub>O<sub>4</sub> exhibits a more intense pre-edge peak than CoO because it contains tetrahedrally coordinated Co<sup>2+</sup> in a non-centrosymmetric environment. Looking back at the pre-edge regions of the Co K-edge XAS spectra for the Ni-Co-O@3D Ni-*x* samples, the pre-edge feature of the Ni-Co-O@3D Ni-*x* samples is very similar to that of CoO, providing evidence for its centrosymmetric (or near centrosymmetric) nature with pure Co<sup>2+</sup> in the octahedral site. Looking further, the intensity of the pre-edge feature of the Ni-Co-O@3D Ni-*x* samples increases with increasing applied voltages that show a slight site symmetry variation from a centrosymmetric to a non-centrosymmetric coordination environment [19].

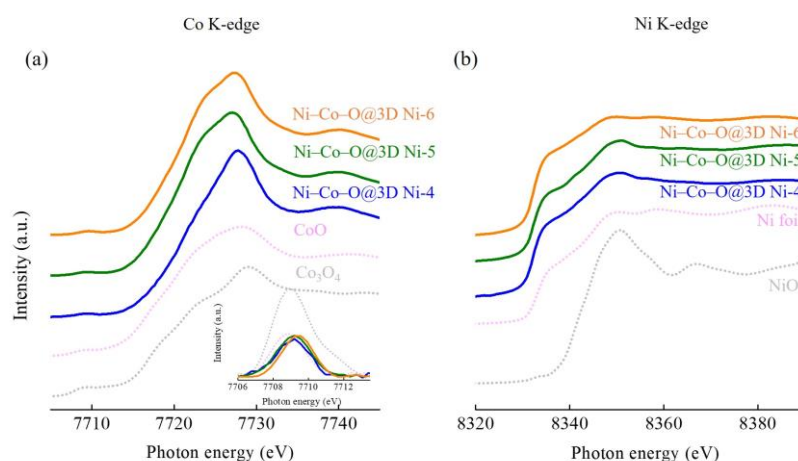
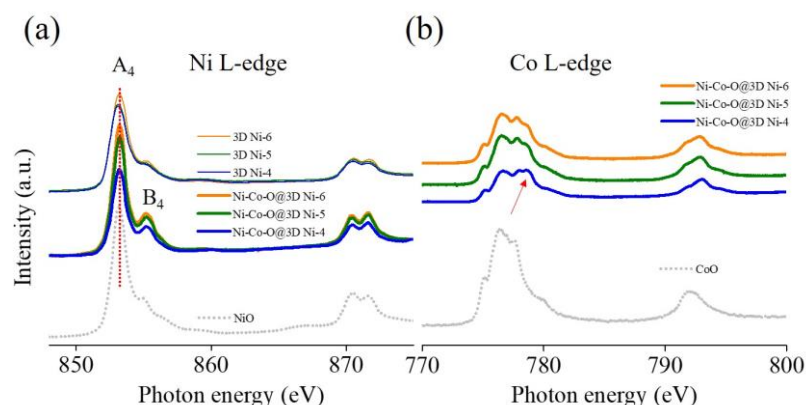


**Figure 4.** (a) Co K-edge and (b) Ni K-edge XAS spectra of Ni-Co-O@3D Ni-*x* samples (*x* = 4, 5, and 6).

The main absorption edge feature in the Co and Ni K-edge XAS spectra originates from the electron transitions from the transition metal 1s to empty 4p states, which are characteristic of octahedral and tetrahedral coordination around Co and Ni sites. In contrast to the standard samples (CoO and Co<sub>3</sub>O<sub>4</sub>), the Co K-edge XAS spectra of the Ni-Co-O@3D Ni-*x* samples correspond to the overlap of the spectra of CoO and Co<sub>3</sub>O<sub>4</sub>. It is believed that the Ni-Co-O@3D Ni-*x* samples exist as a mixture of Co<sup>2+</sup>/Co<sup>3+</sup> in the octahedral–tetrahedral environment. The edge position is close to that of CoO, suggesting that the Ni-Co-O@3D Ni-*x* samples exist in the mixture of the Co<sup>2+</sup>/Co<sup>3+</sup> oxidation state (mainly Co<sup>2+</sup>). However, the spectra clearly show that the edge position is negatively shifted under applied voltages increasing from 4 to 6 V, suggesting a decrease in the oxidation state of Co. Figure 4b shows the Ni K-edge XAS spectra of all Ni-Co-O@3D Ni-*x* samples, and

these spectra are essentially composed of a shoulder and a main absorption feature. By comparing these spectra with reference compounds, it can be seen that all Ni–Co–O@3D Ni-x samples are predominantly in the Ni-metallic state. This may be due to the influence of substrate effects (Ni substrate), which cause a strong substrate background intensity.

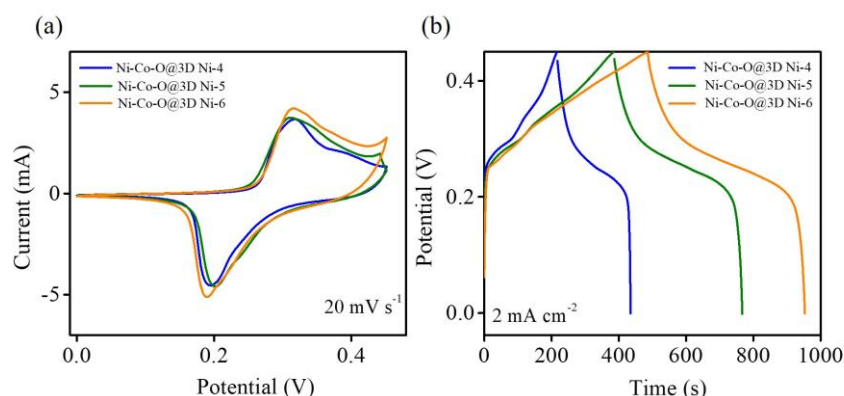
Figure 5a,b show the Ni and Co  $L_{3,2}$ -edge XAS spectra of the 3D Ni-x and Ni–Co–O@3D Ni-x samples. Compared to hard XAS in transmission mode (bulk sensitive), soft XAS in total electron yield (TEY) mode is used in this study as it is more surface-sensitive. Hence, the combination of hard and soft XAS analysis can be used simultaneously to provide complementary information on the source association and a better understanding of the electronic structures around the target materials, which could be further extended to explore the underlying mechanisms involved in electrochemical applications [20]. The Ni and Co L-edge probes the electronic transitions from the 2p core hole to the unoccupied 3d states of Ni and Co. The Ni and Co 2p core hole spin–orbit interaction splits the spectrum into two sections:  $2p_{3/2}$  ( $L_3$ ) and  $2p_{1/2}$  ( $L_2$ ) spectral features. The position and spectral line shape characteristics of these features in the 3d metal  $L_{3,2}$ -edge XAS spectra offer insights into the local atomic and electronic structures of the metal ions, which are directly related to the electronic configuration and oxidation state. The broader  $L_2$  feature compared to the  $L_3$  feature is due to the Coster–Kronig Auger decay process, which spreads out the details of the  $L_2$  feature over a wider energy range. Hence, the  $L_3$  XAS feature, characterised by a double-humped shape, provides clear spectroscopic signals (the double-humped feature) that effectively fingerprint the effects and trends in the  $t_{2g}/e_g$  orbital signatures, the metal oxidation state, and the spin state [21,22]. The Ni  $L_3$  XAS features show that all 3D Ni-x samples are in the  $Ni^{2+}$  oxidation state, which is particularly evident in the case of the 3D Ni-6 samples. During the subsequent hydrothermal growth of Ni-Co oxides, the Ni  $L_3$  XAS features of the Ni–Co–O@3D Ni-x samples exhibit a mixed oxidation state of  $Ni^{2+}$  (labelled  $A_4$ ) and  $Ni^{3+}$  (labelled  $B_4$ ) in contrast to the NiO standard sample and previous studies [21]. The Ni–Co–O@3D Ni-x samples show an increasing trend in the feature area ratio of  $Ni^{2+}$  and  $Ni^{3+}$  in the Ni  $L_3$  XAS analysis with the growth of Ni-Co oxides in the 3D Ni-x samples with increasing applied voltages, while the results show that Ni–Co–O@3D Ni-6 contains the Ni element in a relatively lower oxidation state during the growth of Ni-Co oxides in 3D Ni-6 when a relatively negative voltage is applied. In the Co  $L_3$  XAS features, it is evident that both  $Co^{2+}$  and  $Co^{3+}$  are present in all Ni–Co–O@3D Ni-x samples [22]. Notably, the  $Co^{3+}$  feature (indicated by the red arrow) shows a decreasing trend as the Ni-Co oxides grow on the 3D Ni-x substrates with increasing applied voltages. This suggests that the Ni–Co–O@3D Ni-6 sample may represent Co in a lower oxidation state. From the Ni and Co  $L_{3,2}$ -edge XAS spectra, it can be inferred that the oxidation state of Ni and Co elements in the Ni–Co–O@3D Ni-x samples are influenced by the applied voltages on the 3D Ni-x samples and the subsequent growth of Ni-Co oxides. Thus, it can be concluded that the lower oxidation states of Ni and Co are formed in the Ni–Co–O@3D Ni-6 sample. Additional evidence is provided by the high-resolution XPS spectra of Ni 2p and Co 2p in the Ni–Co–O@3D Ni sample (Figure S3 in the Supplementary Materials). Both the Ni 2p and Co 2p XPS spectra in Figure S3 exhibit two spin-orbit doublets: Ni  $2p_{1/2}/Ni 2p_{3/2}$  and Co  $2p_{1/2}/Co 2p_{3/2}$ . The Ni  $2p_{1/2}$  (Ni  $2p_{3/2}$ ) doublets can be deconvoluted into three peaks located at approximately 872.1 eV (854.4 eV), 873.5 eV (856.2 eV), and 880.0 eV (861.2 eV), which are characteristic of the  $Ni^{2+}$ ,  $Ni^{3+}$ , and shake-up satellite (Sat.), respectively. Similarly, the Co  $2p_{1/2}$  (Co  $2p_{3/2}$ ) doublets can be individually deconvoluted into three peaks located at approximately 796.2 eV (780.9 eV), 794.5 eV (779.4 eV), and 803.1 eV (786.2 eV) corresponding to the  $Co^{2+}$ ,  $Co^{3+}$ , and shake-up satellite (Sat.), respectively [23,24]. These results demonstrate the presence of mixed oxidation states for the Ni ( $Ni^{2+}/Ni^{3+}$ ) and Co ( $Co^{2+}/Co^{3+}$ ) available in the Ni–Co–O@3D Ni sample. Notably, the  $Ni^{2+}(Co^{2+})$  features are more prominent than the  $Ni^{3+}(Co^{3+})$  features, confirming the lower oxidation states of Ni and Co in the Ni–Co–O@3D Ni sample. These results are consistent with the XAS analysis.



**Figure 5.** (a) Ni K-edge and (b) Co L-edge XAS spectra of 3D Ni-*x* and Ni-Co-O@3D Ni-*x* samples (*x* = 4, 5, and 6).

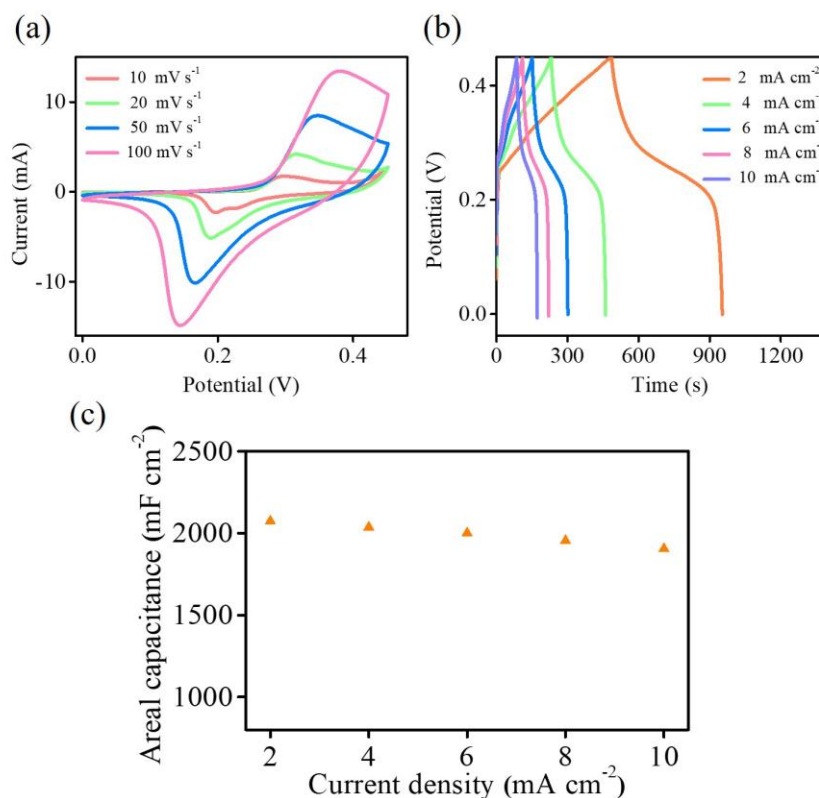
To evaluate the capacitive performance of the Ni-Co-O@3D Ni-*x* samples, cyclic voltammetry (CV) and galvanostatic charge/discharge (GCD) measurements were, in a 1 M KOH solution, within the voltage range of 0.0 to 0.45 V versus Ag/AgCl. Figure 6a illustrates the CV curves of all Ni-Co-O@3D Ni-*x* samples at a scan rate of 20 mV s<sup>-1</sup>, exhibiting a pair of well-defined redox peaks corresponding to the reversible Faradaic redox reactions of Co<sup>2+</sup>/Co<sup>3+</sup> and Ni<sup>2+</sup>/Ni<sup>3+</sup> transitions, indicating an excellent pseudocapacitance performance. A comparison reveals that the CV curve of the Ni-Co-O@3D Ni-6 sample exhibits a larger area than the other two Ni-Co-O@3D Ni-*x* samples, indicating that the Ni-Co-O@3D Ni-6 sample has a much better supercapacitor performance. Figure 6b represents the GCD comparison curve of the Ni-Co-O@3D Ni-*x* samples at a current density of 2 mA cm<sup>-2</sup>. The resulting area capacitance can be calculated using the formula  $C = (I \Delta t) / (A \Delta V)$ , where *C* represents areal capacitance (mF cm<sup>-2</sup>), *I* is the discharge current (mA),  $\Delta t$  is the discharge time (s),  $\Delta V$  is the voltage change during discharge (V), and *A* is the average area of the electrode (cm<sup>2</sup>) (the average area of all working electrodes is 0.0785 cm<sup>2</sup>). The GCD curves of all Ni-Co-O@3D Ni-*x* samples exhibit pseudocapacitance behaviour attributed to the reversible Faradaic redox reactions of the nickel and cobalt species in the Ni-Co-O@3D Ni-*x* samples, which is consistent with the CV curves. It can be observed that the Ni-Co-O@3D Ni-6 sample exhibits the highest areal capacitance (2075.6 mF cm<sup>-2</sup>) compared to both the Ni-Co-O@3D Ni-4 (967.1 mF cm<sup>-2</sup>) and Ni-Co-O@3D Ni-5 (1691.6 mF cm<sup>-2</sup>) samples. The enhanced performance of the Ni-Co-O@3D Ni-6 sample can be attributed to the following factors: (1) The 3D well-designed hierarchical interconnected network between the Ni-Co oxide nanosheets and the 3D porous Ni structures on the Ni wire (3D Ni-6 sample) sandwiched 2–3 layers of Ni-Co-O nanosheets (see Figure 3i). This structure provides numerous open spaces and convenient channels, offering a large specific surface area for enhanced electrocatalytic active sites and facilitating electron/ion transfer characteristics [25]. (2) The synergistic effect of Ni and Co in the Ni-Co-O@3D Ni-6 sample results in multiple oxidation states, enabling various reversible Faradaic redox reactions (Co<sup>2+</sup>/Co<sup>3+</sup> and Ni<sup>2+</sup>/Ni<sup>3+</sup> transitions), which contribute to higher supercapacitive properties [26]. (3) The Ni-Co-O@3D Ni-6 sample has a lower oxidation state of Ni and Co compared to that of the other two Ni-Co-O@3D Ni-*x* samples. This lower oxidation state of Ni and Co undergoes significant changes during the charging and discharging process, further confirming the enhanced capacity performance based on the pseudocapacitive properties dependent on the oxidation state of the as-prepared samples [27].





**Figure 6.** (a) Cyclic voltammetry curve and (b) galvanostatic charge/discharge curve results of Ni-Co-O@3D Ni-*x* samples (*x* = 4, 5, and 6).

To gain further insight into the capacitive performance of the Ni-Co-O@3D Ni-6 sample, Figure 7a,b show the CV curves at various scan rates and GCD curves at various current densities from 0 to 0.45 V. The CV curves maintain their shape, while the peak current increases with increasing scan rates (Figure 7a). Based on the GCD curves (Figure 7b), the areal capacitance reaches a maximum of 2075.6 mF cm<sup>-2</sup> at a current density of 2 mA cm<sup>-2</sup>, and 91.9 % of the areal capacitance (1906.7 mF cm<sup>-2</sup>) is retained even at a current density of 10 mA cm<sup>-2</sup> (Figure 7c). The CV and GCD results in Figure 7 clearly demonstrate the favourable rate capability and pseudocapacitive behaviour of the Ni-Co-O@3D Ni-6 sample. Moreover, the as-synthesized Ni-Co-O@3D Ni sample exhibits comparable or better performance compared to previously reported supercapacitors based on transition metal (Ni or/and Co) compound electrode materials, as summarized in Table 1 [28–33].

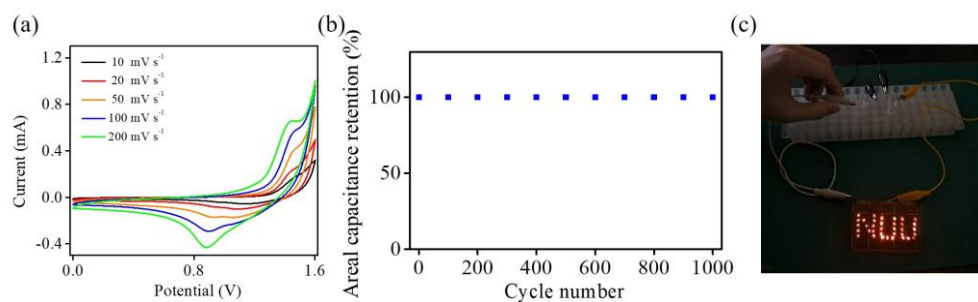


**Figure 7.** (a) Cyclic voltammetry curves of Ni-Co-O@3D Ni-6 at different scan rates, (b) galvanostatic charge/discharge curves of Ni-Co-O@3D Ni-6 at different current densities, and (c) areal capacitance of Ni-Co-O@3D Ni-6 at different current densities.

**Table 1.** Performance comparison of electrochemical supercapacitor based on transition metal (Ni or/and Co) compound electrode materials.

Electrode Materials	Current Density (mA cm <sup>-2</sup> )	Areal Capacitance (mF cm <sup>-2</sup> )	Reference
Co <sub>3</sub> O <sub>4</sub> @NiCo <sub>2</sub> O <sub>4</sub>	3	1330	[28]
Co–Ni layered double hydroxide (LDH)	5	1236	[29]
Co–Ni LDH@zeolitic imidazolate framework-67 (ZIF-67)	1	1979.2	[30]
NiCo <sub>2</sub> O <sub>4</sub> /C	2	1998.2	[31]
NiCo <sub>2</sub> O <sub>4</sub> /C	1	2057	[32]
SnO <sub>2</sub> @NiCo <sub>2</sub> O <sub>4</sub>	1	1490	[33]
Ni–Co–O@3D Ni	2	2075.6	This Work

To further demonstrate the practical usage of the Ni–Co–O@3D Ni-6 sample in a supercapacitor, a solid-state symmetric supercapacitor is fabricated using two as-fabricated Ni–Co–O@3D Ni-6 samples as the positive and negative electrodes with a KOH–PVA gel electrolyte, and it is further tested by CV. Figure 8a shows the CV curves at various scan rates within an operating potential window of 1.6 V. The curves exhibit a pair of redox peaks, indicating the pseudocapacitive nature of the Ni–Co–O@3D Ni-6 samples resulting from Faradaic redox reactions. Importantly, the CV curves of the symmetric supercapacitor retain their characteristic profile without any significant polarization when the potential window reaches 1.6 V, demonstrating ideal capacitive behaviour and good reversibility. This allows the symmetric supercapacitor to operate within a stable electrochemical behaviour in a 1.6 V operating potential window. The long-term cycling performance is a key factor in evaluating supercapacitance for practical application. Figure 8b demonstrates galvanostatic charge/discharge measurements over 1000 cycles at a current density of 10 mA cm<sup>-2</sup> and a wide operating voltage window from 0 to 1.6 V. The result indicates that approximately 100% of the specific capacity is retained after 1000 cycles, indicating excellent cycle stability. To further demonstrate the practical use of the Ni–Co–O@3D Ni-6 sample, two serially connected solid-state symmetric supercapacitors are used to illuminate a parallel National United University (NUU) logo (Figure 8c), consisting of 36 red light-emitting diodes (LEDs). The LEDs illuminate simultaneously, demonstrating the successful operation of the solid-state symmetric supercapacitors. The outstanding capacitive performance highlights the promising practical application of solid-state symmetric supercapacitors assembled with Ni–Co–O@3D Ni-6 samples.

**Figure 8.** (a) Cyclic voltammetry curves of Ni–Co–O@3D Ni-6 solid-state symmetric supercapacitor at different scan rates, (b) cycling test of Ni–Co–O@3D Ni-6 solid-state symmetric supercapacitor, and (c) photograph of LED pattern.

#### 4. Conclusions

In this study, we synthesized Ni–Co–O@3D Ni materials by combining a hydrogen bubble template (3D Ni) and a hydrothermal process (Ni–Co–O@3D Ni). The resulting nanomaterials were then evaluated as binder-free electrodes for supercapacitors. The Ni–Co–O@3D Ni materials possess a well-designed hierarchical interconnected network with 3D structures. The electronic structure and local structural change play a crucial role in the capacitive performance (especially for Ni–Co–O@3D Ni-6). Ni–Co–O@3D Ni-6 is composed of sandwiched layers consisting of 2–3 layers of Ni–Co–O nanosheets. This unique structure provides abundant open spaces and convenient channels, supporting a high density of electroactive sites. Additionally, the synergistic effect of Ni and Co in Ni–Co–O@3D Ni, which exhibit multiple oxidation states, enable various reversible Faradaic redox reactions. This contributes to enhanced electrochemical capacitance ( $2075.6 \text{ mF cm}^{-2}$  at a current density of  $2 \text{ mA cm}^{-2}$ ). To demonstrate practical application, we fabricated a solid-state symmetric supercapacitor using Ni–Co–O@3D Ni-6. The device exhibited excellent cycling stability, retaining approximately 100% capacitance after 1000 cycles. Moreover, we successfully utilized the supercapacitor to illuminate a desired pattern consisting of 36 red LEDs in parallel. These results highlight the excellent capacitive performance of the as-fabricated Ni–Co–O@3D Ni symmetric supercapacitor devices, meeting the requirements for practical applications of supercapacitors.

**Supplementary Materials:** The following supporting information can be downloaded at <https://www.mdpi.com/article/10.3390/en16145467/s1>. Figure S1: XRD of 3D Ni, Ni–Co–O@3D Ni, and Ni–Co–O@3D Ni annealed at  $300 \text{ }^\circ\text{C}$ ; Figure S2: EDX of 3D Ni and Ni–Co–O@3D Ni; Figure S3: High-resolution XPS spectra of Ni 2p and Co 2p of Ni–Co–O@3D Ni.

**Author Contributions:** Conceptualization, H.-W.C. and Y.-C.T.; methodology, H.-W.C., C.-H.L., Y.-X.H., J.-L.C. and J.-M.C.; software, C.-H.L., J.-L.C. and J.-M.C.; formal analysis, C.-H.L. and Y.-X.H.; investigation, H.-W.C., C.-H.L., Y.-X.H., J.-L.C., J.-M.C. and Y.-C.T.; data curation, C.-H.L. and Y.-X.H.; writing—original draft preparation, H.-W.C. and Y.-C.T.; writing—review and editing, H.-W.C. and Y.-C.T.; visualization, H.-W.C.; supervision, H.-W.C.; project administration, H.-W.C. and Y.-C.T. All authors have read and agreed to the published version of the manuscript.

**Funding:** This research was funded by the National Science and Technology Council and National United University, Taiwan (NSTC 112-2221-E-239-001-MY3, NSTC 112-2221-E-005-007-MY3, and MOST 111-2221-E-005-003 and SE112002).

**Data Availability Statement:** Not applicable.

**Acknowledgments:** For instrumentation support, we thank the National Science and Technology Council and the Instrument Center of National Chung Hsing University, Taiwan, for help with FESEM measurements (NSTC 112-2740-M-005-001).

**Conflicts of Interest:** The authors declare no conflict of interest.

#### References

1. Chang, H.-W.; Chen, F.-Y.; Lu, Y.-R.; Huang, Y.-C.; Lin, P.-J.; Tang, M.-T.; Lin, B.-H.; Chou, W.-C.; Dong, C.-L.; Tsai, Y.-C. Preparation and enhanced supercapacitive performance of Ni-Zn-Co-S/3D Ni porous substrate using electrochemical and synchrotron X-ray spectroscopic techniques. *Catal. Today* **2022**, *388*, 47–54. [CrossRef]
2. Kumar, D.R.; Prakasha, K.; Prakash, A.; Shim, J.-J. Direct growth of honeycomb-like  $\text{NiCo}_2\text{O}_4$ @ Ni foam electrode for pouch-type high-performance asymmetric supercapacitor. *J. Alloys Compd.* **2020**, *836*, 155370. [CrossRef]
3. Ali, A.; Hameed, I.; Ammar, M.; Mujahid, R.; Mirza, S. Enhanced rate capability for asymmetric supercapacitors by binder-free Zn-Ni-Co oxide nanoflakes on Ni foam. *J. Energy Storage* **2021**, *37*, 102472. [CrossRef]
4. Naderi, L.; Shahrokhian, S. Nickel molybdate nanorods supported on three-dimensional, porous nickel film coated on copper wire as an advanced binder-free electrode for flexible wire-type asymmetric micro-supercapacitors with enhanced electrochemical performances. *J. Colloid Interface Sci.* **2019**, *542*, 325–338. [CrossRef]
5. Chaudhari, N.K.; Jin, H.; Kim, B.; Lee, K. Nanostructured materials on 3D nickel foam as electrocatalysts for water splitting. *Nanoscale* **2017**, *9*, 12231–12247. [CrossRef] [PubMed]
6. Ni, W.; Wu, H.B.; Wang, B.; Xu, R.; Lou, X.W. One-pot synthesis of ultra-light nickel nanofoams composed of nanowires and their transformation into various functional nanofoams. *Small* **2012**, *8*, 3432–3437. [CrossRef]

7. Wang, T.; Zhao, B.; Jiang, H.; Yang, H.-P.; Zhang, K.; Yuen, M.M.; Fu, X.-Z.; Sun, R.; Wong, C.-P. Electro-deposition of CoNi<sub>2</sub>S<sub>4</sub> flower-like nanosheets on 3D hierarchically porous nickel skeletons with high electrochemical capacitive performance. *J. Mater. Chem. A* **2015**, *3*, 23035–23041. [[CrossRef](#)]
8. Cai, Z.; Bu, X.; Wang, P.; Su, W.; Wei, R.; Ho, J.C.; Yang, J.; Wang, X. Simple and cost effective fabrication of 3D porous core-shell Ni nanochains@NiFe layered double hydroxide nanosheet bifunctional electrocatalysts for overall water splitting. *J. Mater. Chem. A* **2019**, *7*, 21722–21729. [[CrossRef](#)]
9. Kim, J.; Jung, H.; Jung, S.-M.; Hwang, J.; Kim, D.Y.; Lee, N.; Kim, K.-S.; Kwon, H.; Kim, Y.-T.; Han, J.W. Tailoring binding abilities by incorporating oxophilic transition metals on 3D nanostructured Ni arrays for accelerated alkaline hydrogen evolution reaction. *J. Am. Chem. Soc.* **2020**, *143*, 1399–1408. [[CrossRef](#)]
10. Ehsan, M.A.; Ullah, Z.; Nazar, M.F.; Younas, M.; Suliman, M. One step fabrication of nanostructured nickel thin films on porous nickel foam for drastic electrocatalytic oxygen evolution. *Int. J. Hydrogen Energy* **2023**, *48*, 15784–15795. [[CrossRef](#)]
11. Ma, Z.; Zheng, R.; Liu, Y.; Ying, Y.; Shi, W. Carbon nanotubes interpenetrating MOFs-derived Co-Ni-S composite spheres with interconnected architecture for high performance hybrid supercapacitor. *J. Colloid Interface Sci.* **2021**, *602*, 627–635. [[CrossRef](#)] [[PubMed](#)]
12. Swain, N.; Mitra, A.; Saravanakumar, B.; Balasingam, S.K.; Mohanty, S.; Nayak, S.K.; Ramadoss, A. Construction of three-dimensional MnO<sub>2</sub>/Ni network as an efficient electrode material for high performance supercapacitors. *Electrochim. Acta* **2020**, *342*, 136041. [[CrossRef](#)]
13. Biswal, A.; Panda, P.K.; Acharya, A.N.; Mohapatra, S.; Swain, N.; Tripathy, B.C.; Jiang, Z.-T.; Minakshi Sundaram, M. Role of additives in electrochemical deposition of ternary metal oxide microspheres for supercapacitor applications. *Acs Omega* **2020**, *5*, 3405–3417. [[CrossRef](#)]
14. Usman, M.; Ahsan, M.T.; Javed, S.; Ali, Z.; Zhan, Y.; Ahmed, I.; Butt, S.; Islam, M.; Mahmood, A.; Akram, M.A. Facile synthesis of ironnickelcobalt ternary oxide (FNCO) mesoporous nanowires as electrode material for supercapacitor application. *J. Mater.* **2022**, *8*, 221–228.
15. Wang, H.; Zou, W.; Liu, C.; Sun, Y.; Xu, Y.; Sun, W.; Wang, Y.  $\beta$ -ketoenamine-linked covalent organic framework with Co intercalation: Improved lithium-storage properties and mechanism for high-performance lithium-organic batteries. *Batter. Supercaps* **2023**, *6*, e202200434. [[CrossRef](#)]
16. Valdez, R.; Grotjahn, D.B.; Smith, D.K.; Quintana, J.M.; Olivas, A. Nanosheets of Co-(Ni and Fe) layered double hydroxides for electrocatalytic water oxidation reaction. *Int. J. Electrochem. Sci.* **2015**, *10*, 909–918. [[CrossRef](#)]
17. Yu, Y.; Chen, C.; Liu, Y.; Yu, H.; Li, S.; Xue, Y.; Cai, N.; Wang, J.; Yu, F. Hierarchical Ni/Ni(OH)<sub>2</sub>-NiCo<sub>2</sub>O<sub>4</sub> supported on Ni foam as efficient bifunctional electrocatalysts for water splitting. *J. Phys. Chem. C* **2022**, *126*, 5493–5501. [[CrossRef](#)]
18. Yoon, W.-S.; Balasubramanian, M.; Chung, K.Y.; Yang, X.-Q.; McBreen, J.; Grey, C.P.; Fischer, D.A. Investigation of the charge compensation mechanism on the electrochemically Li-Ion deintercalated Li<sub>1-x</sub>Co<sub>1/3</sub>Ni<sub>1/3</sub>Mn<sub>1/3</sub>O<sub>2</sub> electrode system by combination of soft and hard X-ray absorption spectroscopy. *J. Am. Chem. Soc.* **2005**, *127*, 17479–17487. [[CrossRef](#)]
19. Chang, H.-W.; Dong, C.-L.; Lu, Y.-R.; Huang, Y.-C.; Chen, C.-L.; Chen, J.-L.; Chen, J.-M.; Lee, J.-F.; Tsai, Y.-C. Ex-situ soft X-ray absorption spectroscopic investigation of NiCo<sub>2</sub>O<sub>4</sub> annealed in different gases for hydrogen generation by electrolysis of urea. *Int. J. Hydrogen Energy* **2019**, *44*, 15771–15778. [[CrossRef](#)]
20. Ketenoglu, D. A general overview and comparative interpretation on element-specific X-ray spectroscopy techniques: XPS, XAS, and XRS. *X-ray Spectrom.* **2022**; *51*, 422–443.
21. Liang, C.; Zhang, W.; Wei, Z.; Wang, Z.; Wang, Q.; Sun, J. Transition-metal redox evolution and its effect on thermal stability of LiNi<sub>x</sub>Co<sub>y</sub>Mn<sub>z</sub>O<sub>2</sub> based on synchrotron soft X-ray absorption spectroscopy. *J. Energy Chem.* **2021**, *59*, 446–454. [[CrossRef](#)]
22. Guo, M.; Liu, X.; He, R. Restricted active space simulations of the metal L-edge X-ray absorption spectra and resonant inelastic X-ray scattering: Revisiting [Co<sup>II/III</sup>(bpy)<sub>3</sub>]<sup>2+/3+</sup> complexes. *Inorg. Chem. Front.* **2020**, *7*, 1927–1938. [[CrossRef](#)]
23. Bai, R.; Luo, X.; Zhen, D.; Ci, C.; Zhang, J.; Wu, D.; Cao, M.; Liu, Y. Facile fabrication of comb-like porous NiCo<sub>2</sub>O<sub>4</sub> nanoneedles on Ni foam as an advanced electrode for high-performance supercapacitor. *Int. J. Hydrogen Energy* **2020**, *45*, 32343–32354. [[CrossRef](#)]
24. Zhang, G.; Wang, J.; Xie, Y.; Shao, Y.; Ling, Y.; Chen, Y.; Zhang, Y. CoS<sub>2</sub> particles loaded on MOF-derived hollow carbon spheres with enhanced overall water splitting. *Electrochim. Acta* **2023**, *458*, 142511. [[CrossRef](#)]
25. Gao, M.; Li, Y.; Yang, J.; Liu, Y.; Liu, Y.; Zhang, X.; Wu, S.; Cai, K. Nickel-cobalt (oxy)hydroxide battery-type supercapacitor electrode with high mass loading. *Chem. Eng. J.* **2022**, *429*, 132423. [[CrossRef](#)]
26. Zhu, Y.; Huang, H.; Li, G.; Liang, X.; Zhou, W.; Guo, J.; Wei, W.; Tang, S. Graphene-anchored NiCoO<sub>2</sub> nanoarrays as supercapacitor electrode for enhanced electrochemical performance. *Electrochim. Acta* **2017**, *248*, 562–569. [[CrossRef](#)]
27. Wang, Z.; Xu, Z.; Huang, H.; Chu, X.; Xie, Y.; Xiong, D.; Yan, C.; Zhao, H.; Zhang, H.; Yang, W. Unraveling and regulating self-discharge behavior of Ti<sub>3</sub>C<sub>2</sub>T<sub>x</sub> MXene-based supercapacitors. *ACS Nano* **2020**, *14*, 4916–4924. [[CrossRef](#)]
28. Wu, J.; Mi, R.; Li, S.; Guo, P.; Mei, J.; Liu, H.; Lau, W.-M.; Liu, L.-M. Hierarchical three-dimensional NiCo<sub>2</sub>O<sub>4</sub> nanoneedle arrays supported on Ni foam for high-performance supercapacitors. *Rsc Adv.* **2015**, *5*, 25304–25311. [[CrossRef](#)]
29. Lamiel, C.; Hussain, I.; Shim, J.-J. Enhancement of electrochemical performance of nickel cobalt layered double hydroxide@nickel foam with potassium ferricyanide auxiliary electrolyte. *Energy* **2017**, *140*, 901–911. [[CrossRef](#)]
30. Xu, C.; Kong, X.; Zhou, S.; Zheng, B.; Huo, F.; Strømme, M. Interweaving metal-organic framework-templated Co-Ni layered double hydroxide nanocages with nanocellulose and carbon nanotubes to make flexible and foldable electrodes for energy storage devices. *J. Mater. Chem. A* **2018**, *6*, 24050–24057. [[CrossRef](#)]

31. Yang, X.; Mao, L.; Peng, W.; Jin, J.; Yang, S.; Li, G. Synthesis of double-layered NiCo<sub>2</sub>O<sub>4</sub>-nanosheet-loaded PAN/lignin-based hollow carbon nanofibers for high-performance supercapacitor. *ChemistrySelect* **2020**, *5*, 2602–2609. [[CrossRef](#)]
32. Li, Y.; Wang, Q.; Shao, J.; Li, K.; Zhao, W. NiCo<sub>2</sub>O<sub>4</sub>/C core-shell nanoneedles on Ni foam for all-solid-state asymmetric supercapacitors. *ChemistrySelect* **2020**, *5*, 5501–5506. [[CrossRef](#)]
33. He, Y.; Han, W.; Li, L. Hybrid SnO<sub>2</sub>@NiCo<sub>2</sub>O<sub>4</sub> heterostructure with improved capacitive performance. *J. Electron. Mater.* **2020**, *49*, 2419–2428. [[CrossRef](#)]

**Disclaimer/Publisher's Note:** The statements, opinions and data contained in all publications are solely those of the individual author(s) and contributor(s) and not of MDPI and/or the editor(s). MDPI and/or the editor(s) disclaim responsibility for any injury to people or property resulting from any ideas, methods, instructions or products referred to in the content.